XXXVI Ibero-Latin American Congress on Computational Methods in Engineering
CILAMCE
Rio de Janeiro, 22-25 Nov 2015

NONLINEAR ELASTOPLASTIC ANALYSIS OF THIN-WALLED RODS

Yuri Teixeira

Eduardo M. B. Campello

yt@yuriteixeira.arq.br

campello@usp.br

Dept. Structural and Geotechnical Engineering

Polytechnic School, University of So Paulo

P.O. Box 61548, 05424-970, So Paulo, Brazil

Abstract. *In this work, we present the formulation and implementation of a simple elastoplastic constitutive equation for geometrically exact thin-walled rod models. We assume that the plastic deformations may occur due only to the cross-sectional normal stresses, thereby allowing us to work under a simple uniaxial framework. Our approach adopts a standard additive decomposition of the strains together with a linear elastic relation for the elastic part of the deformation. Both ideal plasticity and plasticity with (linear) isotropic hardening are considered. The model is implemented within a finite element thin-walled rod model and is validated by means of numerical examples. We believe that simple elastoplastic models combined with robust thin-walled rod finite elements may be a useful tool for the analysis of thin-walled rod structures, such as, e.g., steel structures.*

Keywords: *Plasticity, Elastoplastic constitutive equation, Thin-walled rods, Finite elements, Steel structures*

1 INTRODUCTION

One of the motivations for the development of scientific research in engineering is the optimization of structural elements with respect to the relation between quantity of material and capacity to perform its function. This greater efficiency is acquired through application of ever more acurate analyses of physical behavior of the structural element in the designed structure. This minimizes the excess of material used to attain the necessary performance and safety. For steel structural elements, one of the biggest barriers to the advance in this area is the complexity of methods of analysis with consideration of geometrical nonlinearity (GNL) and the description of the boundaries of elastic and plastic deformation regimens of the material, i.e. consideration of material nonlinearity (MNL). Given the characteristics of structural steel material and the slender geometry of these elements, effects of GNL and MNL are relevant for many design criteria, most notably in statically indeterminate plane and spatial frames.

The design of structural elements to work in plastic regimen considers resistances greater than those in elastic regimen and allow a gain of efficiency maintaining the necessary safety in design with adequate loading and geometric conditions. This consideration involves the analysis of the structure with partial plastification of the cross-sections as well as, in statically indeterminate structures, the formation of full plastic hinges.

The classical methods of structural analysis with consideration of plasticity and GNL are laborious and have been giving way to analyses with mathematical models that allow a better use of the processing capacity of current computers. The development and implementation of constitutive models with consistent kinematical formulations is, because of that, a subject that has attracted researchers over many recent years.

In this work, we present the formulation and implementation of a simple elastoplastic constitutive equation for geometrically exact thin-walled rod models. We assume that the plastic deformations may occur due only to the cross-sectional normal stresses, thereby allowing us to work under a simple uniaxial framework. Our approach adopts a standard additive decomposition of the strains together with a linear elastic relation for the elastic part of the deformation. Both ideal plasticity and plasticity with (linear) isotropic hardening are considered. The model is implemented within a finite element thin-walled rod model and is validated by means of numerical examples. We believe that simple elastoplastic models combined with robust thin-walled rod finite elements may be a useful tool for the analysis of thin-walled rod structures, such as, e.g., steel structures.

Throughout this text, italic Greek or Latin lowercase letters (a, b, $\ldots$, α, β, $\ldots$) denote scalar quantities, bold italic Greek or Latin lowercase letters ($\boldsymbol{a}$, $\boldsymbol{b}$, $\ldots$, $\boldsymbol{\alpha}$, $\boldsymbol{\beta}$, $\ldots$) denote vectors and bold italic Greek or Latin capital letters ($\boldsymbol{A}$, $\boldsymbol{B}$, $\ldots$) denote second-order tensors in a three-dimensional Euclidean space. Summation convention over repeated indices is adopted, with Greek indices ranging from 1 to 2 and Latin indices from 1 to 3.

2 BRIEF DESCRIPTION OF THE ROD KINEMATICS

This Section outlines the rod kinematical model that we adopt as the basis for our developments. It has origins in the works of Pimenta & Yojo (1993a, 1993b) and was first implemented by Campello (2000). It consists of a geometrically exact formulation in which (i) shear deformation due to bending and (ii) cross-section warping due to combined bending/non-uniform torsion are explicitly taken into account. A straight reference configuration is assumed for the rod axis at the outset. A local orthonormal system $\{\boldsymbol{e}_1^r, \boldsymbol{e}_2^r, \boldsymbol{e}_3^r\}$ with corresponding coordinates $\{x_1, x_2, x_3\}$ is defined in this configuration, with vectors $\boldsymbol{e}_\alpha^r$ ($\alpha = 1, 2$) placed on the rod's cross section and $\boldsymbol{e}_3^r$ placed along the rod axis (see Fig. 1). Points in this configuration are described by the vector field

$$\boldsymbol{\xi} = \boldsymbol{\zeta} + \boldsymbol{a}^r, \tag{1}$$

where $\boldsymbol{\zeta} = x_3 \boldsymbol{e}_3$ describes the position of points at the rod axis and $\boldsymbol{a}^r = x_\alpha \boldsymbol{e}_\alpha$ defines de positions of points at the cross-section relative to the axis. Note that $x_3 \in L = [0, l]$ is the axis coordinate, with l being the rod's reference length.

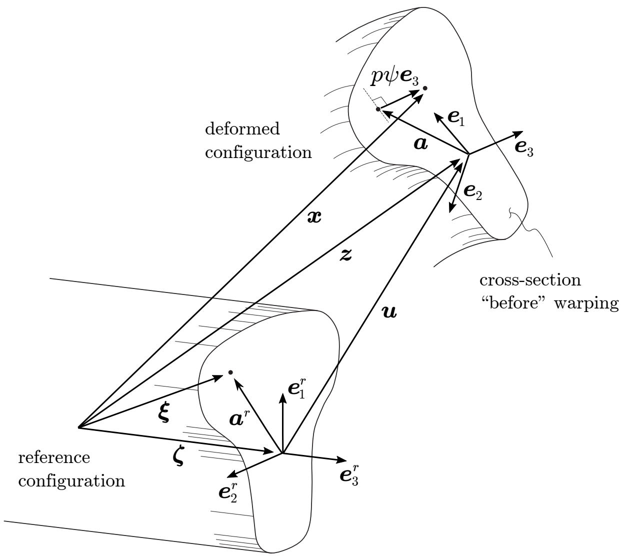

Figure 1: Rod desctiption and kinematics

In the current configuration, another orthonormal system $\{\boldsymbol{e}_1, \boldsymbol{e}_2, \boldsymbol{e}_3\}$ is defined, as depicted in Fig. 1. The deformation of the rod is then described by a vector field $\boldsymbol{x}$ such that the position of the material points is expressed by

$$\boldsymbol{x} = \boldsymbol{z} + \boldsymbol{a} + p\psi \boldsymbol{e}_3, \tag{2}$$

where $\boldsymbol{z} = \hat{\boldsymbol{z}}(x_3)$ describes the position of points at the deformed axis, $\boldsymbol{a} = \hat{\boldsymbol{a}}(x_\alpha, x_3)$ defines the position of points at the deformed cross-section *in the projection of its plane*, $\psi = \hat{\psi}(x_\alpha)$ is a function defining the warping of the cross-section with respect to its shear center (the so-called warping function) and $p = \hat{p}(x_3)$ is a scalar parameter that gives ψ its amplitude.

Many possibilities exist for the choice of ψ, as for example the classical Saint-Venant warping function, the Vlasov sectorial area (Vlasov, 1961), or any other function that adequately describes the out-of-plane deformation of the cross-section. In the present work, we adopt a ψ that is approximated using the finite element method on a bidimensional mesh of the cross-section. In Eq. (2), and from Fig. 1, one finds that $\boldsymbol{z} = \boldsymbol{\zeta} + \boldsymbol{u}$, where $\boldsymbol{u}$ is the displacement vector of points of the rod axis. Vector $\boldsymbol{a}$, in turn, is obtained by $\boldsymbol{a} = \boldsymbol{Q}\boldsymbol{a}^r = x_\alpha \boldsymbol{e}_\alpha$, in which $\boldsymbol{Q}$ is the rotation tensor of the cross-section. Accordingly, no cross-sectional in-plane distortion is allowed, but first order shear deformations are accounted for since $\boldsymbol{a}$ is not necessarily normal to the deformed axis. Relation $\boldsymbol{e}_i = \boldsymbol{Q}\boldsymbol{e}_i$ ($i = 1, 2, 3$) holds for the local systems.

The rotation tensor $\boldsymbol{Q}$ may be written in terms of the Euler rotation vector $\boldsymbol{\theta}$ by means of the well-known Euler-Rodrigues formula

$$\boldsymbol{Q} = \boldsymbol{I} + \frac{\sin\theta}{\theta}\boldsymbol{\Theta} + \frac{1}{2}\frac{\sin^2(\theta/2)}{(\theta/2)^2}\boldsymbol{\Theta}^2, \tag{3}$$

in which $\theta = \|\theta\|$ is the rotation angle of the cross-section and $\boldsymbol{\Theta} = \mathrm{Skew}(\boldsymbol{\theta})$ is the skew-symmetric tensor whose axial vector is $\boldsymbol{\theta}$.

Components of $\boldsymbol{u}$ and $\boldsymbol{\theta}$ on a global Cartesian system along with the scalar parameter p constitute the seven degrees-of-freedom of this rod model. They are grouped into a vector $\boldsymbol{d}$ as follows:

$$\boldsymbol{d} = \begin{bmatrix} \boldsymbol{u} \\ \boldsymbol{\theta} \\ p \end{bmatrix}. \tag{4}$$

The deformation gradient $\boldsymbol{F}$ is obtained from differentiation of Eq. (2) with respect to $\boldsymbol{\xi}$. Using the notation $(\bullet)' = \partial(\bullet)/\partial x_3$ and $(\bullet)_{,\alpha} = \partial(\bullet)/\partial x_\alpha$ for derivatives, it is written as

$$\boldsymbol{F} = \boldsymbol{Q}(\boldsymbol{I} + \psi_{,\alpha} p\boldsymbol{e}_3^r \otimes \boldsymbol{e}_\alpha^r + \boldsymbol{\gamma}_3^r \otimes \boldsymbol{e}_3^r) = \boldsymbol{Q}\boldsymbol{F}^r, \tag{5}$$

where

$$\boldsymbol{\gamma}_3^r = \boldsymbol{\eta}^r + \boldsymbol{\kappa}^r \times (\boldsymbol{a}^r + \psi p\boldsymbol{e}_3^r) + \psi p'\boldsymbol{e}_3^r, \tag{6}$$

in which

$$\boldsymbol{\eta}^r = \boldsymbol{Q}^T\boldsymbol{z}' - \boldsymbol{e}_3^r \quad \text{and} \quad \boldsymbol{\kappa}^r = \boldsymbol{\Gamma}^T\boldsymbol{\theta}'. \tag{7}$$

Vector $\boldsymbol{\gamma}_3^r$ in Eq. (6) can be regarded as the cross-sectional generalized strain vector, with $\boldsymbol{\eta}^r$ and $\boldsymbol{\kappa}^r$ of Eq. (7) being the rod's strains (they encompass the axis elongation and the cross-sectional shear and specific rotations). Tensor $\boldsymbol{\Gamma}$ in Eq. $(7)_2$ reads as

$$\boldsymbol{\Gamma} = \boldsymbol{I} + \frac{1}{2}\frac{\sin^2(\theta/2)}{(\theta/2)^2}\boldsymbol{\Theta} + \frac{1-(\sin\theta)/\theta}{\theta^2}\boldsymbol{\Theta}^2. \tag{8}$$

Linearization of Eq. (5) with respect to $\boldsymbol{d}$ yields the virtual deformation gradient. Using the symbol "δ" to denote linearized or virtual quantities, the result is as follows:

$$\delta\boldsymbol{F} = \delta\boldsymbol{\Omega}\boldsymbol{F} + \boldsymbol{Q}(\psi_{,\alpha}\delta p\boldsymbol{e}_3^r \otimes \boldsymbol{e}_\alpha^r + \delta\boldsymbol{\gamma}_3^r \otimes \boldsymbol{e}_3^r), \tag{9}$$

where $\delta\boldsymbol{\Omega} = \delta\boldsymbol{Q}\boldsymbol{Q}^T$ is a skew-symmetric tensor whose axial vector is denoted by $\delta\boldsymbol{\omega}$. One can show that $\delta\boldsymbol{\omega} = \mathrm{axial}(\delta\boldsymbol{Q}\boldsymbol{Q}^T) = \boldsymbol{\Gamma}\delta\boldsymbol{\theta}$, with $\boldsymbol{\Gamma}$ given by Eq. (8). The virtual strain vector $\delta\boldsymbol{\gamma}_3^r$ of Eq. (9) is obtained from linearization of Eq. (6) and reads as

$$\delta\boldsymbol{\gamma}_3^r = \delta\boldsymbol{\eta}^r + \delta\kappa^r \times (\boldsymbol{a}^r + \psi p\boldsymbol{e}_3^r) + \psi\delta p'\boldsymbol{e}_3^r + \psi\delta p\boldsymbol{\kappa}^r \times \boldsymbol{e}_3^r, \tag{10}$$

in which

$$\delta\boldsymbol{\eta}^r = \boldsymbol{Q}^T(\delta\boldsymbol{u}' + \boldsymbol{Z}'\boldsymbol{\Gamma}\delta\boldsymbol{\theta}) \quad \text{and} \quad \delta\boldsymbol{\kappa}^r = \boldsymbol{Q}^T(\boldsymbol{\Gamma}'\delta\boldsymbol{\theta} + \boldsymbol{\Gamma}\delta\boldsymbol{\theta}') \tag{11}$$

are obtained from the linearization of Eq. (7). In the above expressions, $\boldsymbol{Z}'$ is the skew-symmetric tensor whose axial vector is $\boldsymbol{z}'$, i.e. $\boldsymbol{Z}' = \mathrm{Skew}(\mathrm{z}')$.

Let now the first Piola-Kirchhoff stress tensor be expressed in terms of its column-vectors as

$$\boldsymbol{P} = \boldsymbol{\tau}_i \otimes \boldsymbol{e}_i^r. \tag{12}$$

Vectors $\boldsymbol{\tau}_i$ are the nominal stresses acting on a point of the rod according to planes whose normals in the reference configuration are $\boldsymbol{e}_i^r$. One may also write $\boldsymbol{P} = \boldsymbol{Q}\boldsymbol{P}^r$, with

$$\boldsymbol{P}^r = \boldsymbol{\tau}_i^r \otimes \boldsymbol{e}_i^r \tag{13}$$

as the back-rotated counterpart of $\boldsymbol{P}$. In this case, vectors $\boldsymbol{\tau}_i^r$ are the back-rotated stress vectors.

The internal virtual work of the rod, with the aid of Eqs. (9) and (12), is given by

$$\delta W_{int} = \int_L \int_A (\boldsymbol{P} : \delta \boldsymbol{F})\, dA\, dL = \int_L (\boldsymbol{\sigma}^r \cdot \delta \boldsymbol{\varepsilon}^r)\, dL, \tag{14}$$

where A is the area of the cross-sections at the reference configuration and

$$\boldsymbol{\sigma}^r = \begin{bmatrix} \boldsymbol{n}^r & \boldsymbol{m}^r & Q & B \end{bmatrix}^T \quad \text{and} \quad \delta\boldsymbol{\varepsilon}^r = \begin{bmatrix} \delta\boldsymbol{\eta}^r & \delta\boldsymbol{\kappa}^r & \delta p & \delta p' \end{bmatrix}^T \tag{15}$$

are 8×1 vectors grouping the cross-sectional stress resultants and their corresponding virtual strains, which show up when integration over A is performed in Eq. (14). These stress resultants are given by

$$\begin{aligned} \boldsymbol{n}^r &= \int_A \boldsymbol{\tau}_3^r\, dA = V_\alpha \boldsymbol{e}_\alpha^r + N\boldsymbol{e}_3^r \\ \boldsymbol{m}^r &= \int_A (\boldsymbol{a}^r + \psi p \boldsymbol{e}_3^r) \times \boldsymbol{\tau}_3^r\, dA = M_\alpha \boldsymbol{e}_\alpha^r + T\boldsymbol{e}_3^r \\ Q &= \int_A ((\boldsymbol{\tau}_\alpha^r \cdot \boldsymbol{e}_3^r)\psi_{,\alpha} + \boldsymbol{\tau}_3^r \cdot (\boldsymbol{\kappa}^r \times \boldsymbol{e}_3^r)\psi)\, dA \\ B &= \int_A (\boldsymbol{\tau}_3^r \cdot \boldsymbol{e}_3^r)\psi\, dA. \end{aligned} \tag{16}$$

Components of the first two vectors above are the resultant shear forces (V_α), normal force (N), bending moments (M_α) and torsional moment (T) of the cross-sections, whereas Q and B are the so-called bi-shear and bi-moment due to the consideration of warping.

Vector $\delta\boldsymbol{\varepsilon}^r$ of Eq. (15), in view of Eq. (11), may be written as $\delta\boldsymbol{\varepsilon}^r = \boldsymbol{\Psi}\boldsymbol{\Delta}\delta\boldsymbol{d}$, where

$$\boldsymbol{\Psi} = \begin{bmatrix} \boldsymbol{Q}^T & \boldsymbol{Q}^T\boldsymbol{Z}'\boldsymbol{\Gamma} & \boldsymbol{O} & \boldsymbol{o} & \boldsymbol{o} \\ \boldsymbol{O} & \boldsymbol{Q}^T\boldsymbol{\Gamma}' & \boldsymbol{Q}^T\boldsymbol{\Gamma} & \boldsymbol{o} & \boldsymbol{o} \\ \boldsymbol{o}^T & \boldsymbol{o}^T & \boldsymbol{o}^T & 1 & 0 \\ \boldsymbol{o}^T & \boldsymbol{o}^T & \boldsymbol{o}^T & 0 & 1 \end{bmatrix} \quad \text{and} \quad \boldsymbol{\Delta} = \begin{bmatrix} \boldsymbol{I}\frac{\partial}{\partial x_3} & \boldsymbol{O} & \boldsymbol{O} & \boldsymbol{o} & \boldsymbol{o} \\ \boldsymbol{O} & \boldsymbol{I} & \boldsymbol{I}\frac{\partial}{\partial x_3} & \boldsymbol{o} & \boldsymbol{o} \\ \boldsymbol{o}^T & \boldsymbol{o}^T & \boldsymbol{o}^T & 1 & \boldsymbol{I}\frac{\partial}{\partial x_3} \end{bmatrix}^T. \tag{17}$$

The external virtual work of the rod is given by

$$\delta W_{ext} = \int_L \left(\int_C \bar{\boldsymbol{t}} \cdot \delta \boldsymbol{x} \, dC + \int_A \bar{\boldsymbol{b}} \cdot \delta \boldsymbol{x} \, dA \right) dL = \int_L (\bar{\boldsymbol{q}} \cdot \delta \boldsymbol{d}) \, dL, \tag{18}$$

in which $\bar{\boldsymbol{t}}$ is the external surface traction acting on the rod's surface per unit reference area, C is the contour of the cross-sections, and $\bar{\boldsymbol{b}}$ is the vector of external body forces per unit reference volume. With $\delta \boldsymbol{x}$ above given from linearization of Eq. (2), evaluation of the contour and area integrals in Eq. (18) renders the external force resultants, which are grouped into vector $\bar{\boldsymbol{q}}$ as shown below:

$$\bar{\boldsymbol{q}} = \begin{bmatrix} \bar{\boldsymbol{n}} \\ \boldsymbol{\Gamma}^T \bar{\boldsymbol{m}} \\ \bar{B} \end{bmatrix}, \quad \text{where} \quad \begin{aligned} \bar{\boldsymbol{n}} &= \int_C \bar{\boldsymbol{t}} \, dC + \int_A \bar{\boldsymbol{b}} \, dA \\ \bar{\boldsymbol{m}} &= \int_C (\boldsymbol{a} + \psi p \boldsymbol{e}_3) \times \bar{\boldsymbol{t}} \, dC + \int_A (\boldsymbol{a} + \psi p \boldsymbol{e}_3) \times \bar{\boldsymbol{b}} \, dA \\ \bar{B} &= \int_C \psi \bar{\boldsymbol{t}} \cdot \boldsymbol{e}_3 \, dC + \int_A \psi \bar{\boldsymbol{b}} \boldsymbol{e}_3 \, dA. \end{aligned} \tag{19}$$

Components of $\bar{\boldsymbol{n}}$ and $\bar{\boldsymbol{m}}$ are respectively the resultant external forces and moments, whereas $\bar{B}$ is the resultant external bi-moment, all per unit reference length of the rod axis.

The equilibrium of the rod is enforced by means of the virtual work theorem in a standard way:

$$\delta W = \delta W_{int} - \delta W_{ext} = 0 \quad \text{in } L, \quad \forall \delta \boldsymbol{d} \mid \delta \boldsymbol{d}(0) = \delta \boldsymbol{d}(l) = \boldsymbol{o}, \tag{20}$$

with δW_{int} and δW_{ext} given by Eqs. (14) and (18). The Fréchet derivative of the above weak form with respect to $\boldsymbol{d}$ leads to the tangent formulation of this model:

$$\delta(\delta W) = \int_L \left((\boldsymbol{\Psi \Delta} \delta \boldsymbol{d}) \cdot (\boldsymbol{D \Psi \Delta} \delta \boldsymbol{d}) + (\boldsymbol{\Delta} \delta \boldsymbol{d}) \cdot (\boldsymbol{G \Delta} \delta \boldsymbol{d}) - (\delta \boldsymbol{d} \cdot \boldsymbol{L} \delta \boldsymbol{d}) \right) dL, \tag{21}$$

in which

$$\boldsymbol{D} = \frac{\partial \boldsymbol{\sigma}^r}{\partial \boldsymbol{\varepsilon}^r}, \qquad \boldsymbol{G} = \frac{\partial \boldsymbol{\Psi}^T \boldsymbol{\sigma}^r}{\partial (\boldsymbol{\Delta d})} \qquad \text{and} \qquad \boldsymbol{L} = \frac{\partial \bar{\boldsymbol{q}}}{\partial \boldsymbol{d}}. \tag{22}$$

Explicit expressions for $\boldsymbol{D}$, $\boldsymbol{G}$ and $\boldsymbol{L}$ above can be found in Pimenta & Yojo (1993) and Campello (2000) (although with a different notation) and will be ommited here. They represent the constitutive effects, the geometric effects of the internal forces and the geometric effects of the external loading on the tangent operator.

3 ELASTOPLASTIC CONSTITUTIVE EQUATION

3.1 Model for small strains

We assume that the inelastic material behavior of the rod is described by the classical elastoplastic constitutive model for small strains. Accordingly, the cross-sectional strain vector $\boldsymbol{\gamma}_3^r$ of Eq. (6) is decomposed additively as

$$\boldsymbol{\gamma}_3^r = \boldsymbol{\gamma}_3^{r|e} + \boldsymbol{\gamma}_3^{r|p}. \tag{23}$$

Furthermore, the plastic strain $\boldsymbol{\gamma}_3^{r|p}$ is assumed to occur due only to the cross-sectional normal stress τ_{33}^r from Eq. (13). This allows us to work under a simple uniaxial framework for the plastic deformations. With these deformation components and considering the linear elastic relation of the Kirchhoff-St. Venant material, we formulate the elastic stress-strain relationship governing τ_{33}^r and $\gamma_{33}^{r|e}$ as

$$\tau_{3\alpha}^r = \tau_{\alpha 3}^r = G(\gamma_{3\alpha}^r + p\psi_{,\alpha}) \tag{24}$$

$$\tau_{33}^r = E\gamma_{33}^{r|e} = E(\gamma_{33}^r - \gamma_{33}^{r|p}) \tag{25}$$

where τ_{33}^r and $\tau_{3\alpha}^r$ are the components of $\boldsymbol{\tau}_3^r$ and correspond to the cross-sectional normal and shear stresses respectively.

For small strains, the back-rotated first Piola-Kirchhoff stress tensor $\boldsymbol{P}^r$ collapses to the second Piola-Kirchhoff stress tensor $\boldsymbol{S}$. And the energy conjugate of $\boldsymbol{S}$ is the Green strain tensor $\boldsymbol{E}$ which, up to the first order is

$$\boldsymbol{E} = \frac{1}{2}(\boldsymbol{F}^T\boldsymbol{F} - \boldsymbol{I}) = \frac{1}{2}\begin{bmatrix} 0 & 0 & \gamma_{31}^r + p\psi_{,1} \\ 0 & 0 & \gamma_{32}^r + p\psi_{,2} \\ \gamma_{31}^r + p\psi_{,2} & \gamma_{32}^r + p\psi_{,2} & 2\gamma_{33}^r \end{bmatrix} \tag{26}$$

where $\gamma_{3\alpha}^r$ and γ_{33}^r are the components of $\boldsymbol{\gamma}_3^r$.

Considering linear isotropic hardening of the material, the admissible stresses for this component lie within the following conditions:

$$\mathcal{F}(\tau_{33}^r, \alpha) = |\tau_{33}^r| - (\sigma_Y + K\alpha) \leq 0 \quad \text{and} \quad \alpha \geq 0 \tag{27}$$

where $\mathcal{F}$ is the yield criterion, σ_Y is the initial yield stress, α is the internal hardening variable and K is the plastic modulus. We adopt an associative plastic flow rule and a simple evolutionary equation for the hardening variable as equivalent plastic strain given by

$$\dot{\gamma}_{33}^{r\,p} = \dot{\alpha}\hat{n} \quad \text{and} \quad \dot{\alpha} = |\dot{\gamma}_{33}^{r\,p}| \quad \text{where} \quad \hat{n} = \frac{\partial \mathcal{F}}{\partial \tau_{33}^r} \tag{28}$$

The Kuhn-Tucker loading/unloading conditions and the consistency condition are then expressed as

$$\mathcal{F} \leq 0, \qquad \dot{\alpha} \geq 0, \qquad \dot{\alpha}\mathcal{F} = 0 \qquad \text{and} \qquad \dot{\alpha}\dot{\mathcal{F}} = 0 \tag{29}$$

With these conditions it is possible to characterize the material behavior in the elastic and plastic states when subject to loading or unloading:

$$\text{elastic}: \begin{cases} \text{loading}: & \mathcal{F} < 0, \quad \dot{\mathcal{F}} > 0, \quad \dot{\alpha} = 0 \\ \text{unloading}: & \mathcal{F} < 0, \quad \dot{\mathcal{F}} < 0, \quad \dot{\alpha} = 0 \end{cases}$$

$$\text{plastic}: \begin{cases} \text{loading}: & \mathcal{F} = 0, \quad \dot{\mathcal{F}} = 0, \quad \dot{\alpha} > 0 \\ \text{unloading}: & \mathcal{F} = 0, \quad \dot{\mathcal{F}} < 0, \quad \dot{\alpha} = 0 \end{cases}$$

To implement this constitutive model within the kinematics described in the previous section, we recover the internal virtual work from Eqs. (10), (11) and (14) and write it in terms of $\boldsymbol{\tau}_i^r$ and $\delta\boldsymbol{\gamma}_3^r$:

$$\begin{aligned}\delta W_{int} &= \int_L \int_A (\boldsymbol{P} : \delta\boldsymbol{F})\, dA\, dL \\ &= \int_L \int_A \tau_{\alpha 3}^r\, \delta\gamma_{\alpha 3}^r + \boldsymbol{\tau}_3^r \cdot (\delta\boldsymbol{\eta}^r + \delta\boldsymbol{\kappa}^r \times (\boldsymbol{a}^r + \psi p \boldsymbol{e}_3^r) + \psi \delta p' \boldsymbol{e}_3^r + \psi \delta p \boldsymbol{\kappa}^r \times \boldsymbol{e}_3^r)\ dA\, dL \\ &= \int_L \int_A \tau_{\alpha 3}^r\, \delta\gamma_{\alpha 3}^r + \boldsymbol{\tau}_3^r \cdot \delta\boldsymbol{\gamma}_3^r\ dA\, dL \end{aligned} \tag{30}$$

3.2 Stress integration algorithm

To implement the stress integration algorithm, specifically the well-known return mapping algorithm for the uni-dimensional case (Simo & Hughes, 1998), we replace the stress, strain and hardening rates by finite increments. It allows us to perform the analysis using an incremental loading scheme.

At the start of the analysis, variables for the hardening and plastic strains are initialized and have their history stored to be used in later steps. We compute the elastic trial stress $\tau_{33n+1}^{r\ trial}$ as part of the same finite element models of Campello & Lago (2014) and described in section 2 and Eq. (30). From this stress component we compute $\mathcal{F}$ and verify the compliance with the yield criterion. Here, the hardening variable from the previous step must be provided:

$$\tau_{33n+1}^{r\ trial} = E(\gamma_{33\,n+1}^r - \gamma_{33\ n}^{r|p}) \tag{31}$$

$$\mathcal{F}_{n+1}^{trial} = |\tau_{33n+1}^{r\ trial}| - (\sigma_Y + K\alpha_n) \tag{32}$$

If $\mathcal{F}_{n+1}^{trial} \leq 0$, the model is either in elastic state or in neutral loading, and the stress and strain are effectively the trials computed. The hardening variables do not change in this case. However, if the yield criterion is not fulfilled, the trial stress is projected to the yield surface and the plastic strain and hardening variables are incremented:

$$\Delta\alpha = \frac{\mathcal{F}_{n+1}^{trial}}{E+K} \quad \text{if} \quad \mathcal{F}_{n+1}^{trial} > 0, \quad \text{else} \quad \Delta\alpha = 0, \tag{33}$$

$$\gamma_{33\ n+1}^{r|p} = \gamma_{33\ n}^{r|p} + \hat{n}\Delta\alpha \quad \text{with} \quad \hat{n} = \frac{\tau_{33n+1}^{r\ trial}}{|\tau_{33n+1}^{r\ trial}|}, \tag{34}$$

$$\alpha_{n+1} = \alpha_n + \Delta\alpha, \tag{35}$$

$$\tau_{33\,n+1}^r = E(\gamma_{33\,n+1}^r - \gamma_{33\ n+1}^{r|p}). \tag{36}$$

3.3 Integration over the cross-section

To compute the stress resultants of Eq. (16), the integration over the cross-section is needed and it cannot be performed analitically because of the progressive plastification of the cross-section. For this implementation, the procedures described above are broken down into a series of steps to account for this integration and also to provide an adequate model for partial plastification of the cross-sections of the rod. As seen in Eq. (6), the dependence of $\boldsymbol{\gamma}_3^r$ on coordinates over the cross-section is gathered in the vector $\boldsymbol{a}^r = x_\alpha \boldsymbol{e}_\alpha$. For this elastoplastic constitutive model, we use an integration scheme similar to that in Campello & Lago (2014). The integration over the cross-section is approximated numerically using a 2-dimensional mesh.

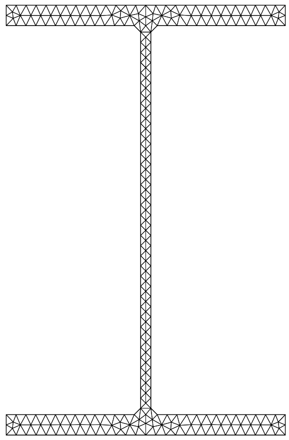

Figure 2: Triangular cross-sectional mesh.

For every cell of this cross-sectional mesh we compute the quantities that depend on $\boldsymbol{a}^r$ using the coodinates of the midpoint and weight this contribution with the area s of the cell.

$$\int_A (\bullet)\, dA \simeq \sum_A (\bullet) s \tag{37}$$

The stress integration algorithm above is then applied to components τ_{33}^r and γ_{33}^r of the stress and strain vectors and to the internal hardening α and plastic strain $\gamma_{33}^{r|p}$ for each of these cells. After that, the tangent matrix and residuum vector can be assembled as in the elastic model.

The warping function used in this implementation is obtained exactly by employing the finite element method using the cross-sectional mesh to solve the following variational problem

$$\int_A \nabla v \cdot \nabla \psi \, dA - \int_A \nabla v \cdot \boldsymbol{g} \, dA = 0 \quad \text{where} \quad \boldsymbol{g} = \begin{bmatrix} 0 & 1 \\ -1 & 0 \end{bmatrix} \boldsymbol{a}^r, \tag{38}$$

v is a test function and ψ is the warping function. We assume that ψ remains unchanged in the plastic deformation regimen.

4 NUMERICAL EXAMPLES

The formulation presented in the previous Section was implemented in the finite element models of the works of Pimenta & Yojo (1993a, 1993b), Campello (2000), Campello & Pimenta (2001) and Campello Lago (2014). Both 2-node and 3-node rod elements (linear and quadratic interpolation functions for all degrees-of-freedom of Eq. (4)) were considered. To resolve the constitutive equation, computation of the stress resultants of Eq. (16) was performed via integration over the cross-section as mentioned. Reduced Gaussian quadrature was used for integration over the rod's length. A Newton incremental/iterative solution scheme is adopted.

We performed several numerical tests in order to validate the implementation. We analyzed examples involving compression, bending, torsion and warping. The results obtained were excellent and compared very well with reference solutions whenever these were available (both in nodal solution and in stress resultants). For the sake of simplicity, we show here the results of only a few of these tests.

For all examples, a triangle mesh is used for the cross-section. The results over the cross-section correspond, on the axis, to the nearest quadrature point in cases of results on the middle or the end of the rod. To improve the approximation of these results, the axis mesh is refined around the critical cross-section. These results are for the formulation without warping of the cross-section. Results with warping cross-sections and reference solutions are being prepared and will be ready in the near future.

4.1 Biarticulated beam

This example adopts a simple shape for the cross-section and was used to validate the implementation through its development. Its constant width produces a more gradual distribution of the stress along the height and thus a noticeably gradual plastification of the cross-section.

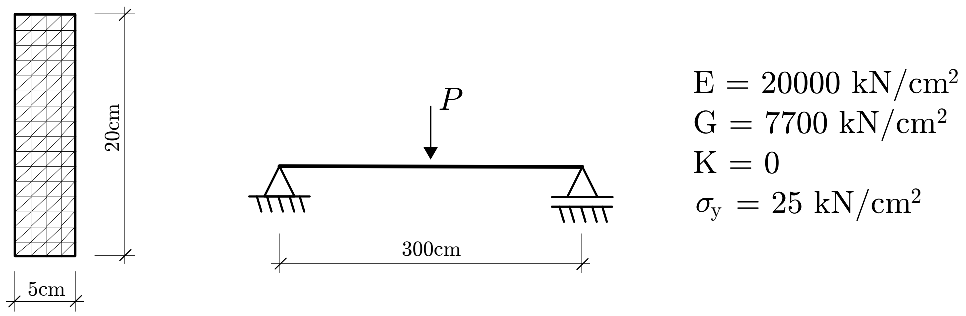

Figure 3: Rod section, boundary conditions and parameters.

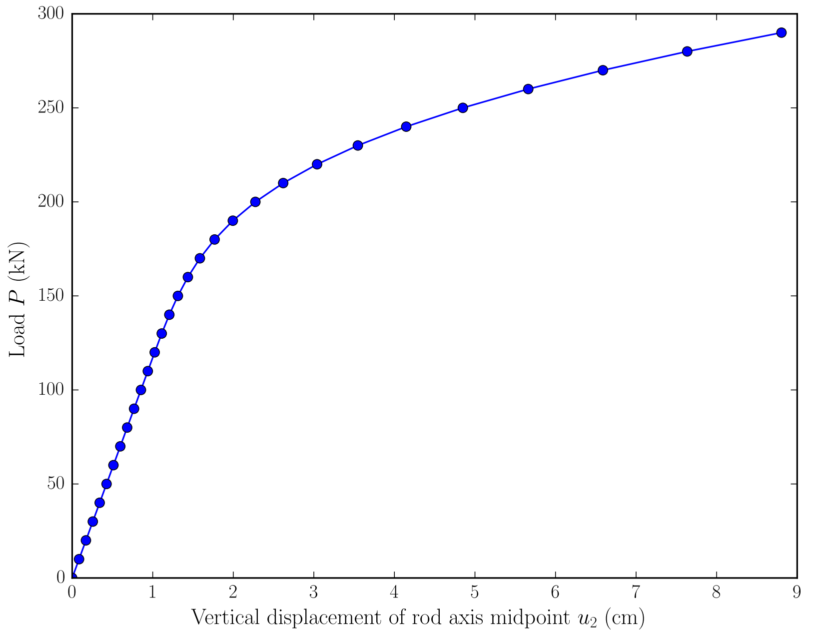

Figure 4: Load $\times$ displacement curve for the midpoint of the rod.

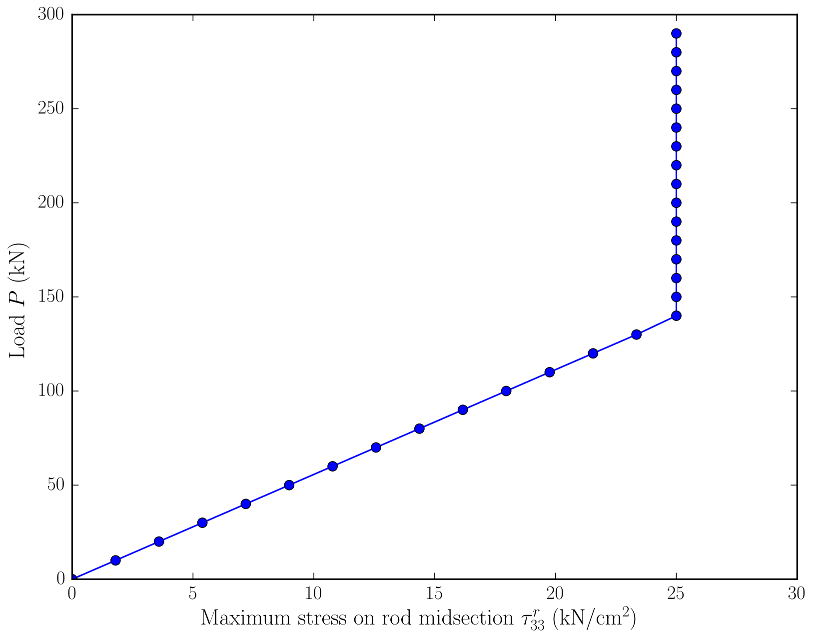

Figure 5: Load $\times$ stress curve for the cross-section that contains the quadrature point closest to the middle of the rod.

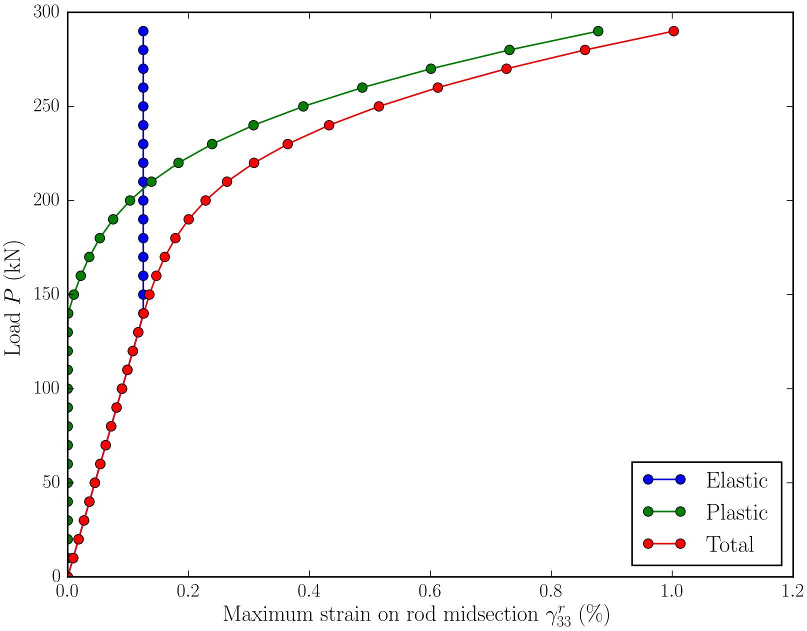

Figure 6: Load × strain curves for elastic, plastic and total strains.

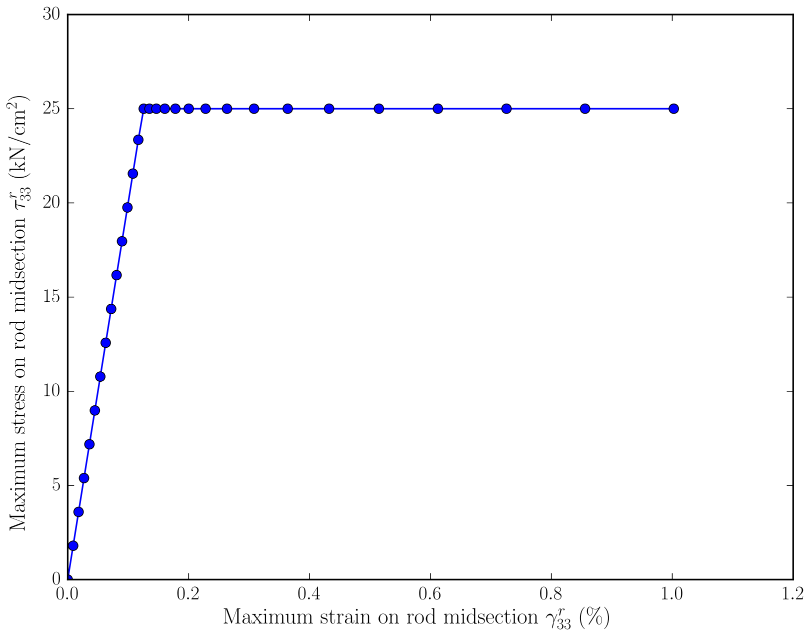

Figure 7: Stress × strain curve as expected for ideal plasticity.

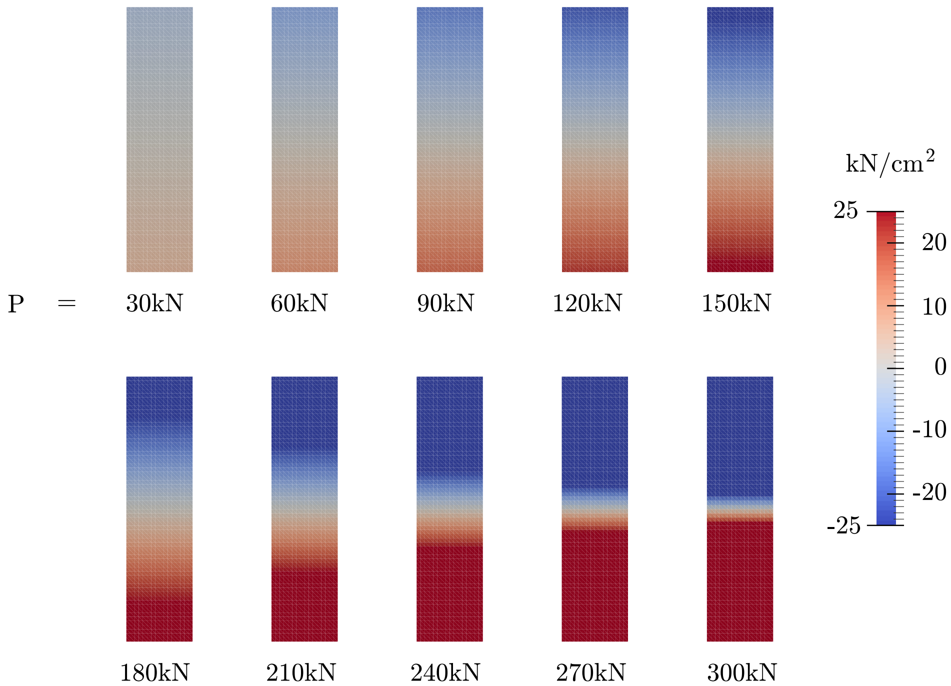

Figure 8: Cross-sectional normal stress τ^r_{33} close to the rod midsection for increasing load.

4.2 Cantilever beam

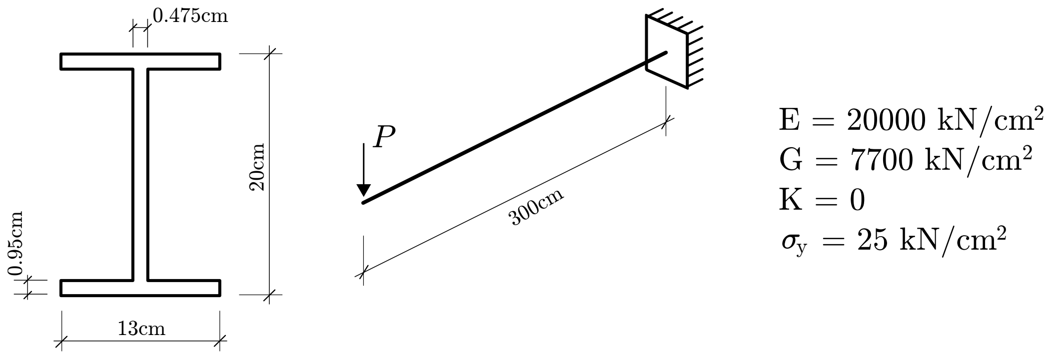

Figure 9: Rod section, boundary conditions and parameters.

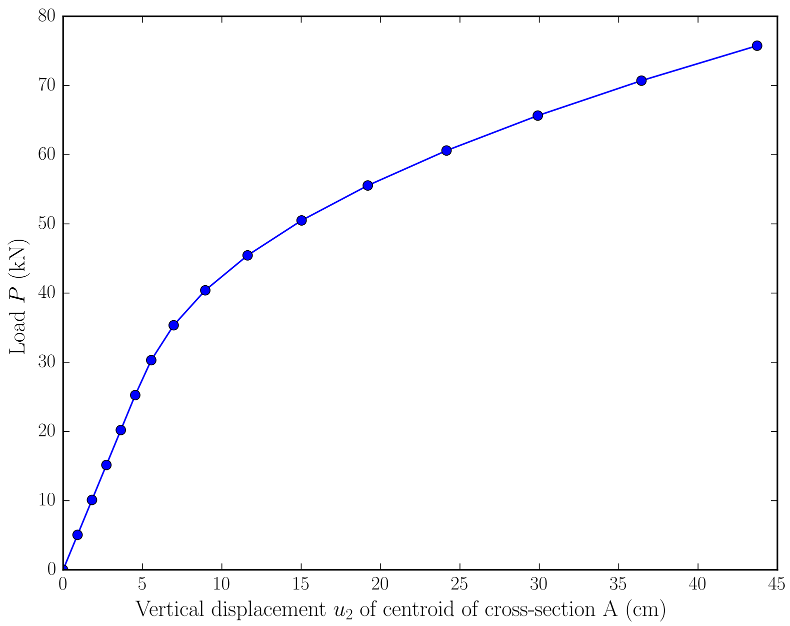

Figure 10: Load $\times$ displacement curve for the free end of the rod.

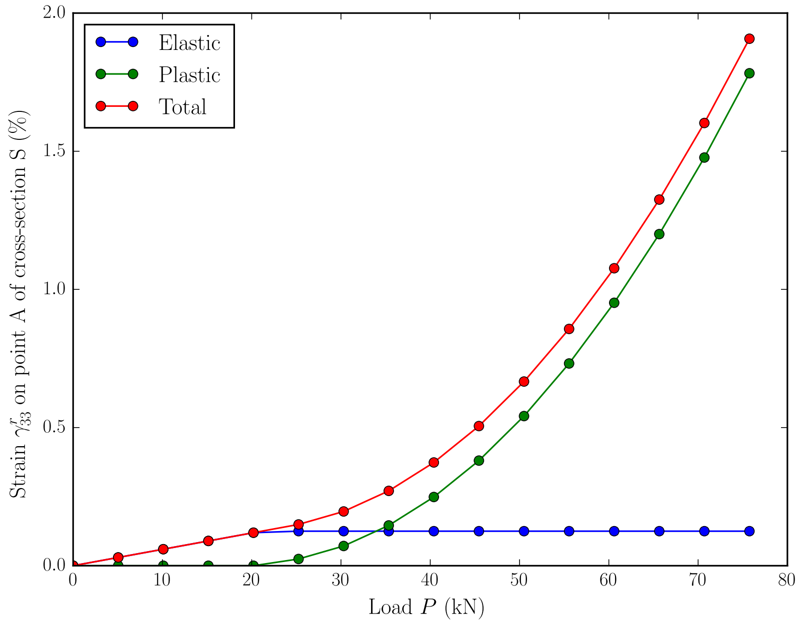

Figure 11: Load $\times$ strain curves for elastic, plastic and total strains.

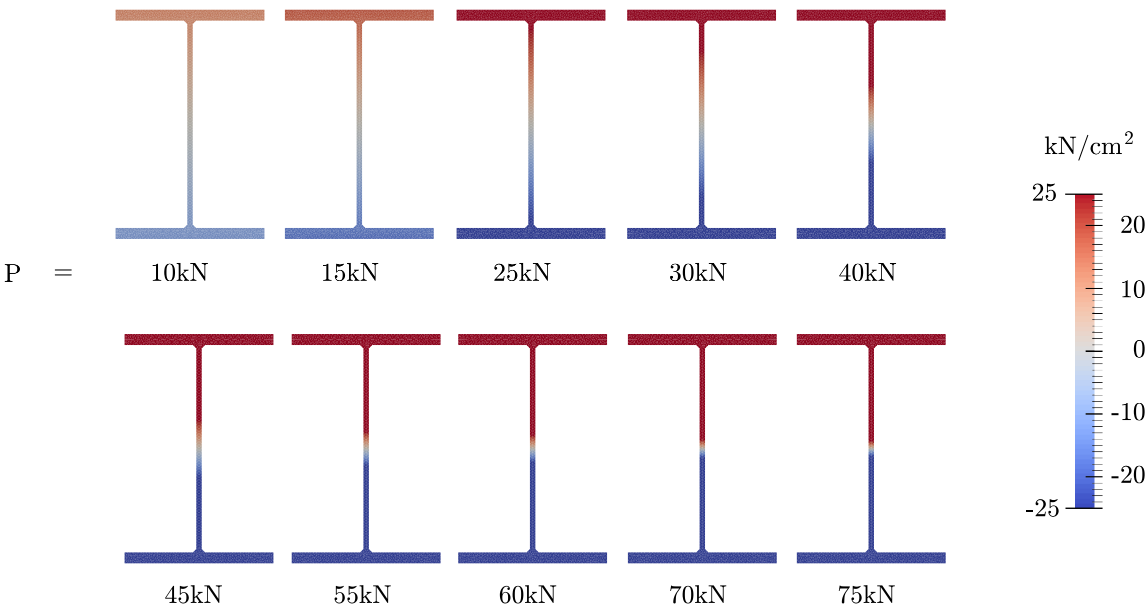

Figure 12: Cross-sectional normal stress τ^r_{33} close to the clamped end for increasing load.

4.3 Doubly clamped beam

This example is of interest to show the asymetric plastification of the middle cross-section, whose neutral line is above the geometric center.

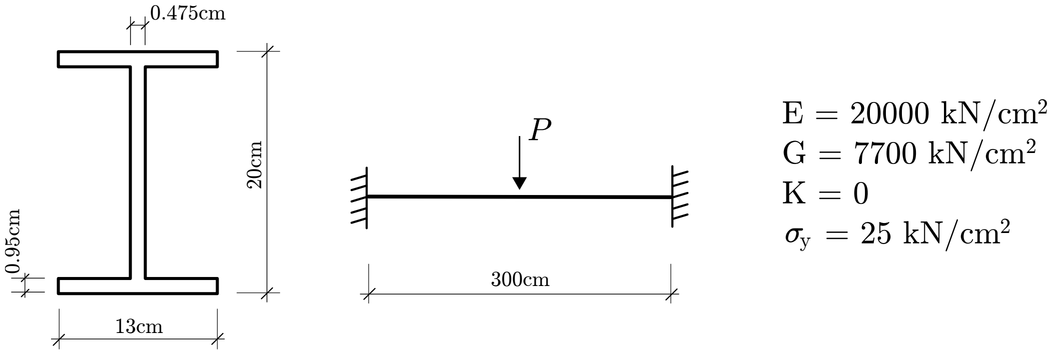

Figure 13: Rod section, boundary conditions and parameters.

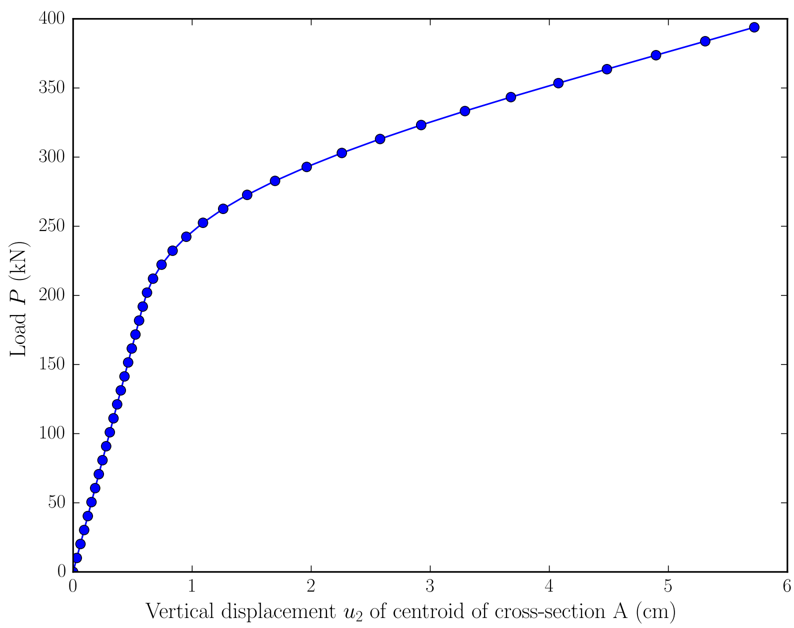

Figure 14: Load $\times$ displacement curve for the midpoint of the rod.

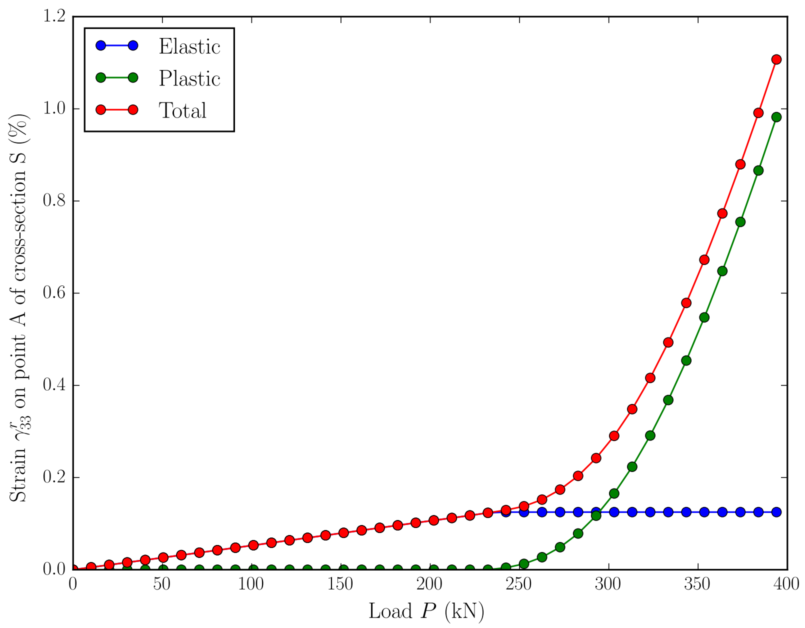

Figure 15: Load $\times$ strain curves for elastic, plastic and total strains.

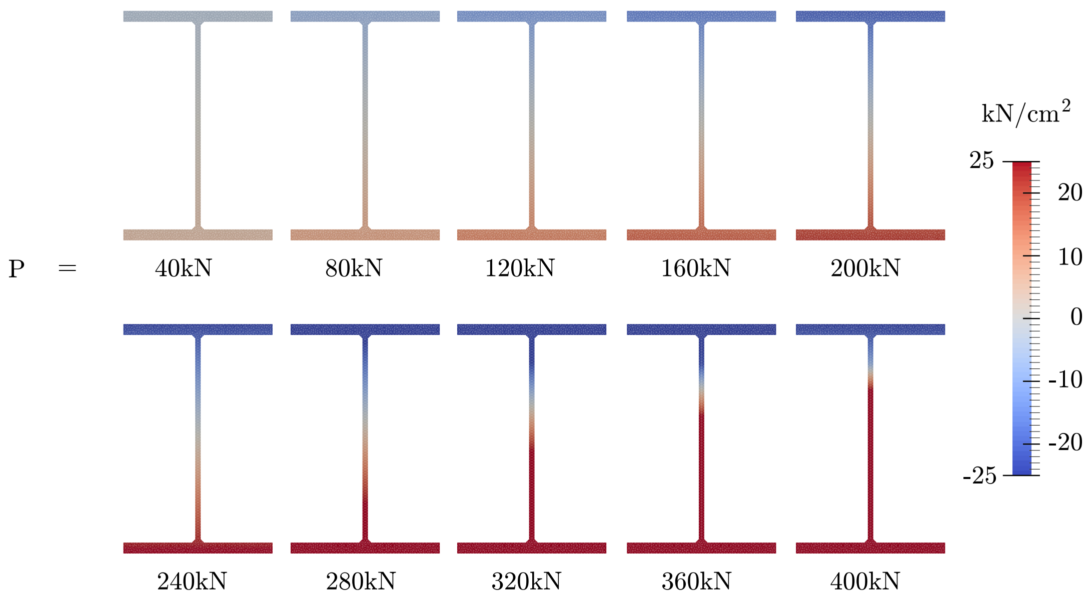

Figure 16: Cross-sectional normal stress τ^r_{33} close to the rod midsection for increasing load.

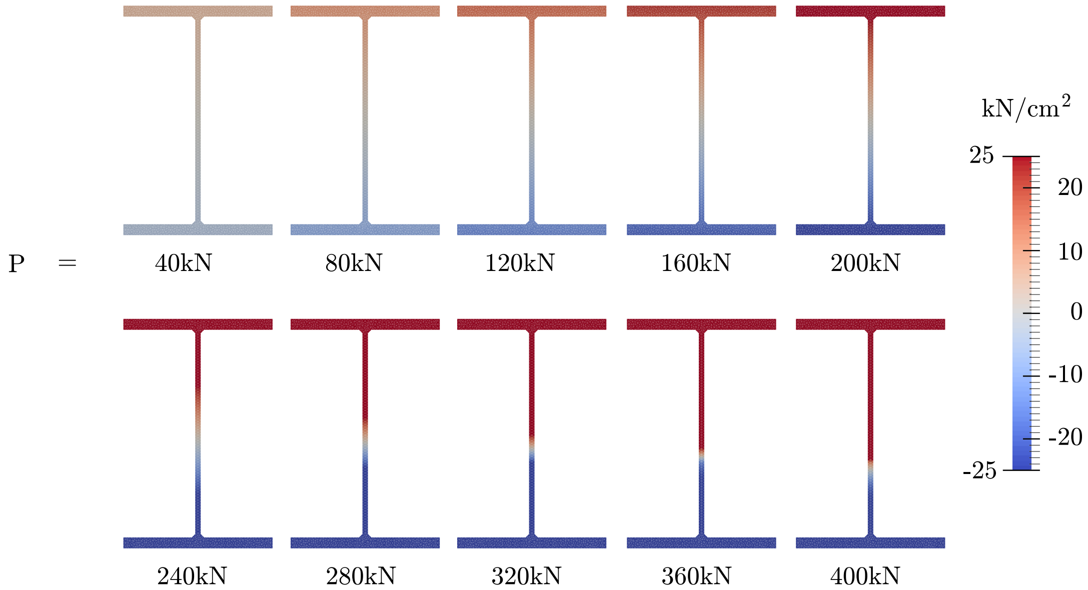

Figure 17: Cross-sectional normal stress τ^r_{33} close to the rod midsection for increasing load.

5 Conclusions

This work presented the formulation and implementation of an elastoplastic constitutive model for geometrically exact rod models under small strains. Preliminary tests showed consistency of the formulation with results from the classical strength of materials. Further testing is necessary to show coherence with models of higher geometric dimensions and with spatial frame models. Future developments include the implementation of warping and distortion of the cross-sectional plane and the analysis of convergence and adaptivety through axial and cross-sectional mesh refinements.

ACKNOWLEDGEMENTS

First author acknowledges CAPES (Brazilian Agency of Graduate Education from Ministry of Education) for the research grant given through the Graduate Program in Civil Engineering of the Polytechnic School of the University of São Paulo.

Second author acknowledges CNPq (Conselho Nacional de Desenvolvimento Cientfico e Tecnolgico) for the research grant 303793/2012-0.

REFERENCES

Campello, E. M. B., 2000. *Nonlinear Analysis of cold-formed steel members*. Dissertation (in Portuguese). Department of Structural and Geotechnical Engineering, University of So Paulo.

Campello, E. M. B., Lago, L. B., 2014. Effect of higher order constitutive terms on the elastic buckling of thin-walled rods. Thin Walled Structures 77:8-16.

Campello, E. M. B., Pimenta, P. M., 2001. Geometrically nonlinear analysis of thin-walled space frames. In: *Proceedings of the Second European Conference on Computational Mechanics (II ECCM)*. Cracow, 2001.

Pimenta, P. M., Yojo, T., 1993a. Geometrically exact analysis of spatial frames. *Applied Mechanics Reviews*, vol. 46, n. 11, part 2, pp. 118–28.

Pimenta, P. M., Yojo, T., 1993b. Geometrically exact analysis of spatial frames with consideration of torsion warping. In: *Proceedings of the XVI Iberian-Latin-American Congress on Computational Methods in Engineering (XVI CILAMCE)*, So Paulo, 1993, pp. 21-30.

Simo, J. C., Hughes, T. J. R., 1998. Computational Inelasticity. ...

Simo, J. C., Vu-Quoc, L., 1986. A three-dimensional finite strain rod model. Part II: Computational Aspects. Comput Methods Appl Mech Eng 58:79-116.

Simo, J. C., Vu-Quoc, L., 1991. A geometrically exact rod model incorporating shear and torsion-warping deformation. Int J Solid Structures 27:371-93.

Vlasov, V. Z., 1961. *Thin-walled elastic beams*. Jerusalem, Israel. Program for Scientific Translation.